Pergamon

Int. J. Heat Mass Transfer. Vol. 40, No. 5, pp. 1083–1094, 1997

0017–9310/97 $17.00+0.00

PII: S0017–9310(96)00152–4

A microscopic thermal model for dry sliding contact

P. CHANTRENNE and M. RAYNAUD

INSA de LYON, Centre de Thermique, URA CNRS 1372, Bâtiment 404-20, Avenue Albert Einstein, 69621 Villeurbanne Cedex France

(*Received* 22 *March* 1994 *and in final form* 25 *April* 1996)

Abstract—A microscopic thermal model for dry sliding contact that accounts for a volume generation of the friction heat is proposed. A numerical procedure that allows the determination of the two parameters α and R_{sl} of macroscopic thermal models for dry sliding contact is given. The results are compared in the case of a simple contact geometry, with an analytical solution for α and R_{sl}. The influences of the microscopic parameters, the contact geometry and the velocity on the two macroscopic parameters are shown. Copyright © 1996 Elsevier Science Ltd.

1. INTRODUCTION

Friction occurs in a lot of mechanisms, like gears, ball bearings, in engines, transmission equipments, brakes and so on. In some cases, the energy dissipation is useful, in others it is not. The determination of the temperature field of a mechanical system, where friction occurs between several parts, is a difficult task and has been tackled for many years for engineering applications. In the case of non-lubricated contact, different macroscopic thermal contact models have been proposed for rubbing interfaces.

At first, it was assumed that the thermal contact is perfect [1–4], thus the temperature of both surfaces in contact is equal. This model is the easiest to use but is limited in applications which do not need accuracy. In other works [5–7], a partition coefficient p is defined; it is assumed that a part, p, of the friction heat, φ_g, goes into one solid while the remaining part goes into the other solid. This model is convenient because the two solids are not coupled and only one parameter, p, must be fixed to calculate the whole temperature fields, but the partition coefficient must be estimated for each particular case, because it depends on the boundary conditions, the material properties and the macroscopic geometry of the two contacting solids.

Actually, perfect contact never exists and, to model this situation, a thermal contact resistance is used. Figure 1 recalls the definition of the thermal contact resistance: when two solids are pressed together the unperfectly smooth surfaces limit the real contact to small areas (Fig. 1a). The conductivity of the interstitial fluid being usually smaller by one or two orders of magnitude than the solid conductivities, the temperature field near the interface is perturbated. Let R_p be the thermal resistance for the perfect contact case, then with the notation of Fig. 1b:

$$R_p = \frac{(T_2 - T_1')}{\varphi}. \tag{1}$$

If the same heat flux density φ goes through the real contact then R_t, the thermal resistance for the real contact (temperature variation given by the thick curve on Fig. 1b), is equal to:

$$R_t = \frac{(T_2 - T_1)}{\varphi}. \tag{2}$$

The static thermal contact resistance represents the perturbation induced by the asperities, it is defined as the difference between R_t and R_p:

$$R_{st} = R_t - R_p. \tag{3}$$

One can also write:

$$R_{st} = \frac{(\theta_2 - \theta_1)}{\varphi} \tag{4}$$

where θ_2 and θ_1 are the extrapolated temperatures in the solids 2 and 1, respectively, at the theoretical geometric interface.

Many numerical [8–10] and experimental [11–13] works were carried out to determine the thermal resistance for static contacts in steady [14, 15] and transient [16, 17] states. The concept of thermal resistance has later been extended to sliding contacts and was experimentally determined in some particular cases [18, 19].

Another model, introduced by Bardon [20], is based on a sliding contact resistance, R_{sl} and another parameter, α, called 'heat generation coefficient'. Bardon's analysis of the contact led to the contact model shown in Fig. 2a. The heat flux is generated at the contact interface and the asperities are modeled with thermal resistances as shown by Fig. 2b: R_{a1} is the solid 1 asperity thermal resistance, R_{c1} and R_{c2} are the constriction thermal resistances and R_i the thermal

NOMENCLATURE

a	thermal diffusivity [$m^2 s^{-1}$]
$2b$	width of asperity [m]
$2B$	periodicity of asperity [m]
cp	specific heat [$J kg^{-1} K^{-1}$]
f	constriction coefficient
g	fraction of the total friction heat being generated in the solid 1
h	thickness of the heat flux generation zone [m]
H	height of the asperity [m]
k	conductivity [$W m^{-1} K^{-1}$]
p	friction heat partition coefficient
r	thermal resistance ratio
R	thermal resistance [$m^2 KW^{-1}$]
T	temperature [K]
V	sliding velocity [$m s^{-1}$]
V_2^*	non-dimensional sliding velocity $V_2^* = 2BV/a_2$.

Greek symbols

α	heat generation coefficient
φ	heat flux density [$W m^{-2}$]
θ	extrapolated temperature at the contact interface [K]
ρ	density [$kg m^{-3}$].

Subscripts

a	asperity
g	generation
i	interstitial fluid or index
p	perfect contact
t	total
c	constriction
st	static contact
sl	sliding contact
1	solid 1
2	solid 2.

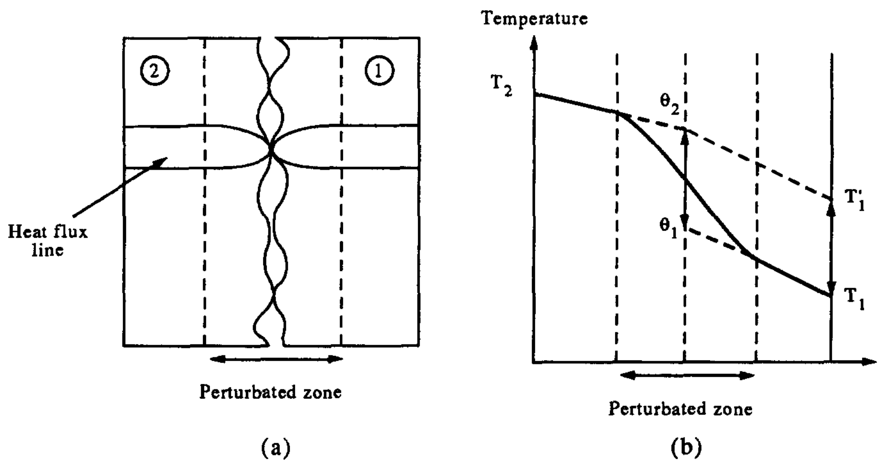

Fig. 1. Illustration of the thermal contact resistance effect.

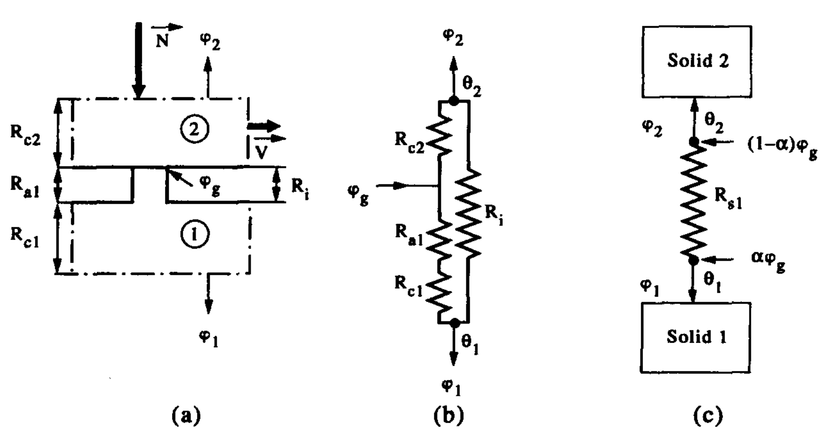

Fig. 2. Bardon's thermal sliding contact model.

resistance due to the interstitial medium. For most cases the constriction resistance is a very local phenomenon since the ratio of the real contact area on the apparent contact area is small and the conductivity of the interstitial medium is much smaller than the solid conductivities. Thus it can be assumed that there is no interaction between the constriction resistance and the interstitial medium resistance. Bardon proposed replacing this four parameters model by the two parameters model shown in Fig. 2c. The four resistances are replaced by a single resistance R_{sl} and it is assumed that a fraction, α, of the heat flux is generated at the surface of the solid 1 while the complementary fraction is generated on the solid 2 surface. The comparison of the resistance scheme of Fig. 2b and c leads [20] to the following expressions for R_{sl} and α:

$$\frac{1}{R_{sl}} = \frac{1}{R_i} + \frac{1}{(R_{c1}+R_{a1}+R_{c2})} \tag{5}$$

$$\alpha = \frac{R_{c2}}{(R_{c1}+R_{a1}+R_{c2})} = \frac{R_{sl2}}{R_{sl1}+R_{sl2}}. \tag{6}$$

Equation (6) shows that, contrary to the partition coefficient, p, α depends on the interface rugosities and thermal properties, on the sliding velocity, but not on the external boundary conditions and macroscopic geometries.

Laraqui [21] proposed another macroscopic model with asperities on the two contacting surfaces. The total height of the asperities is supposed to be constant, so $R_{a2}+R_{a1} = R_a$ is constant, but the position of the contact interface is supposed to vary with a Gaussian distribution. Since it is also assumed that the heat flux is generated at the contact interface, φ_g follows the same Gaussian distribution as the contact interface location. This model also involves two parameters, R_m and R_σ, which correspond to the maximum and the standard deviation of the Gaussian curve, respectively. Except for the perturbated zone, the temperature fields calculated by these two last models are identical.

The assumption of heat generated at the interface of contact is, to our point of view, not realistic. Our analysis, confirmed by many thorough personal communications with tribologists and physicists, has led us to believe that the friction heat generation is a volume phenomenon. Heat is generated by two main means: adhesion which gives rise directly to heat dissipation in the first atomic layers of the contacting surfaces and elastoplastic deformations which release heat in the surrounding contacting volume. The importance of the latter depends on the material properties, surface roughness, contact pressure and velocity. It can represent 5–95% of the friction heat [22].

The first objective of this paper is to present a finer model in which the heat is generated in a volume right under the contact interface. This model has two weaknesses. First it will be shown that it involves many parameters which are not presently all well known. Secondly, it is a microscopic model that cannot be used for macroscopic calculations without a high computational time. The second objective of this work is to present a methodology that enables the calculation of the two macroscopic parameters α and R_{sl} of the macroscopic model proposed by Bardon from this new microscopic model.

The paper is divided into four parts. The microscopic model is described first and applied to a particular contact geometry. An analytical expression for α and R_{sl} is given; then a numerical solution is used to calculate the complete temperature field and the methodology which allows the determination of α and R_{sl} is developed. Finally, a sensitivity analysis of α and R_{sl} to the microscopic parameters, velocity and thermal properties is carried out.

2. CONTACT MODEL

In this model it is assumed that the friction heat is generated within a volume underneath the real contact interface. This is, to our knowledge, the first time that such a volume heat generation is considered.

The contact geometry, schematically represented in Fig. 3, studied by Vullierme *et al.* [18], is considered. This is a comprehension geometry which allows one to understand easily the effect of various parameters. The solid 2 of thickness e_2 has a perfectly smooth surface. The surface of the solid 1 is modelized with periodic asperities. The spatial periodicity is $2B$, the height and the width are equal to H and $2b$, respectively. The total thickness of the solid 1 is e_1. The two solids are supposed to be infinite in the x and z directions. The problem is bi-dimensional and the periodicity allows the study of only an elementary part of this system.

Based on the work of Sadhal [23], the radiation exchange within the cavities formed by the contacting asperities are neglected. The contact at the interface is supposed to be perfect, so the surface temperature asperities are equal. Actually, the contact interface is never perfect due to the existence of nano-asperities. However since they are much smaller than the micro-asperities which are modelized herein, they are neglected [24]. The external surfaces exchange heat by convection with the surroundings. Such boundary condition is used because, if the calculation leads to isothermal external surfaces, it means that the distances e_1 and e_2 chosen were large enough. This is the best way to be sure that the perturbated zone's height is smaller than the studied zone's height, i.e. the heat flux lines are not disturbed by these boundaries. If a temperature or a heat flux were imposed on the external surfaces, we would have to take larger values of e_1 and e_2, for example e_1 and e_2 greater than $2B$, to be sure not to influence the constriction resistances. The heat transfer coefficients and reference temperatures are h_{c1}, T_{in1} and h_{c2}, T_{in2} for the solids 1 and 2, respectively. The cavity formed by the asperity is empty, so

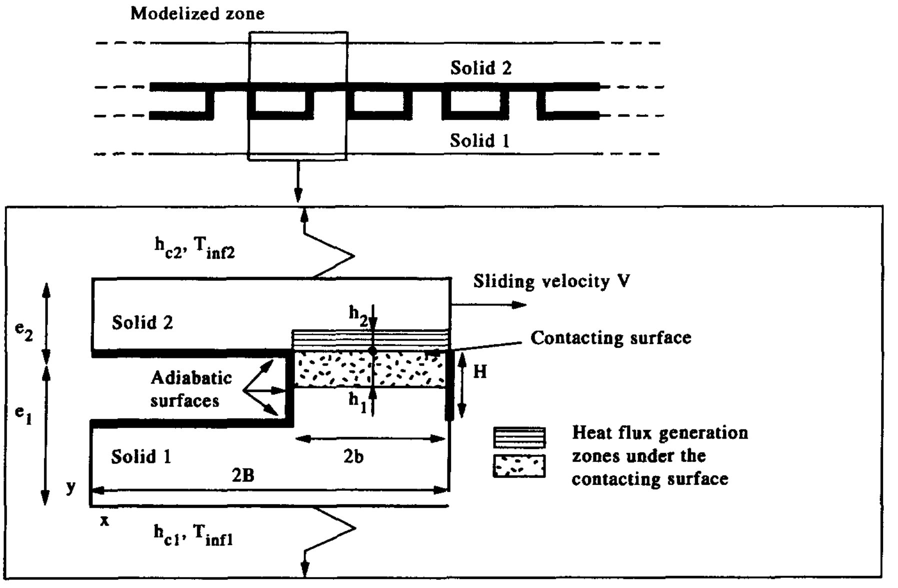

Fig. 3. Microscopic thermal model and geometry studied.

that there is no conductive or convective exchange in this region. Vullierme *et al.* [18] considered a cavity filled with grease where only conduction occurs. This model was used to study the sliding velocity effects on the thermal resistance. Experimental results were in good agreement with numerical results. It showed that the interstitial fluid has a great influence on the contact heat transfer, but since it is not our objective to study these phenomena in this paper, adiabatic cavity surfaces are considered, i.e. R_i tends to infinity. For simplicity and to allow the comparison between the analytical and numerical solutions, the thermophysical properties of the two solids are constants.

The relative velocity between the two solids is noted V. In the remainder of the paper, the solid 1 is considered fixed while the solid 2 slides on it in the direction x, with the velocity V. Herein, the friction heat, φ_g, is not calculated from the velocity, the contact area, the friction coefficient and the normal pressure. A nonzero value is simply taken so as to simulate a heat source. Heat is dissipated within the volume h_2^* $2b$ in the solid 2 underneath the contact and within the volume $h_1^* 2b$ in the asperity of the solid 1. In the most general case, two functions, g_1 and g_2 are introduced to characterize the distribution of the heat generation in each solid. In the most simple case, g_1 and g_2 are constant, thus a fraction g of the friction heat is dissipated in the solid 1 and the complementary part 1-g in the solid 2. As it will be shown, g is different either from p and α. The thermal resistance network that corresponds to this microscopic model is shown in Fig. 4a. This microscopic model involves three thermal resistances, the two lengths h_1 and h_2 and the two heat source distribution functions g_1 and g_2.

3. ANALYTICAL DETERMINATION OF α AND R_{SL}

The aim of this section is to obtain analytical expressions of the two macroscopic thermal contact model parameters from the previous microscopic model (Fig. 4a). These relations will be used to interpret the results of the sensitivity study obtained with the numerical method to determine α and R_{sl}.

3.1. *Analytical expression of* R_{sl}

All the calculations are done for an apparent contact area of unity, i.e. a length of unity is taken in the z direction and $1/2B$ periods are considered in the x direction. Thus all of the thermal resistances are in m^2 K W^{-1}.

Since the case of an infinite interstitial thermal resistance R_i, is considered, equation (5) reduces to:

$$R_{sl} = R_{a1} + R_{c1} + R_{c2} = R_{sl1} + R_{sl2}. \quad (7)$$

According to Bardon [20], the thermal resistance due to solid 1 is considered as a static resistance which does not depend on the sliding velocity. In previous studies [25, 26], it was shown that the static constriction resistance varies linearly with $1/k$ so:

$$R_{c1} = f_{c1} \frac{2B}{k_1} \quad (8)$$

where f_{c1} is the constriction coefficient which depends on the geometry. Based on an electric analogy, experimental values of f_{c1} were given for circular contact area by Bardon and Cordier [27], while Carlslaw and Jaeger [28] and Yovanovich [29] determined the analytical expressions for the circular contact area case and for the elliptical contact area case, respectively.

With the parameters defined (Fig. 3) and using the definition of the thermal contact resistance, the thermal resistance due to the asperity R_{a1} can be calculated:

$$R_{a1} = \left(\frac{B}{b} - 1\right)\frac{H}{k_1} = f_{a1}\frac{H}{k_1}. \quad (9)$$

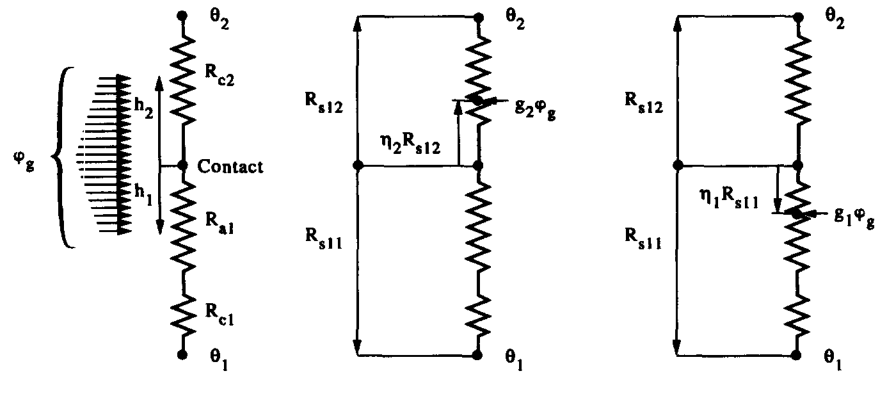

Fig. 4. (a) Thermal resistance network for the new microscopic model with a volume heat generation. The volume generation is considered as the superposition of local surface heat generation in the solid 1 (b) and in the solid 1 (c).

Using equations (8) and (9), one can write the expression of the thermal contact resistance due to the solid 1:

$$R_{s11} = \left(\frac{H}{2B} f_{a1} + f_{c1}\right)\frac{2B}{k_1} = f_1 \frac{2B}{k_1}. \qquad (10)$$

Since the solid 2 is flat: $R_{s12} = R_{c2}$. According to Bardon [20], the sliding resistance is equal to the static resistance multiplied by a function of the non-dimensional sliding velocity V_2^*. Since the static constriction resistance varies linearly with $1/k$, the thermal sliding contact resistance of the solid 2 can be expressed as:

$$R_{s12} = f_2 \frac{2B}{k_2} F_2(V_2^*). \qquad (11)$$

Actually, the non-dimensional sliding velocity is the Peclet number calculated with the sliding velocity and the characteristic length $2B$ [18]: $V_2^* = 2V_2B/a_2$. The spatial periodicity of the asperities, $2B$, is used as the characteristic length even if the contact length $2b$ seems to be a more important parameter for the constriction resistance. As a matter of fact, machine part surfaces are usually ridged and the periodicity of the ridges is easily measured with a profilometer. On the other hand the length $2b$, which represents the real contact area, depends on the mechanical properties and the contact pressure; it is then much more difficult to obtain. The Peclet number represents the ratio of the heat convected away due to the sliding motion, to the heat diffusion in the solid 2. $F_2(V_2^*)$ is equal to 1 when V_2^* is equal to zero and tends to zero when V_2^* tends to infinity. If V_2^* is infinite, the temperature field in the solid 2 is one-dimensional in the y direction and is not perturbated by the asperity, which implies that R_{s12} equals zero. Thus, for the particular case of infinite velocity the total sliding contact resistance is only equal to the resistance induced by the static solid:

$$R_{s1}(V_2^* \to \infty) = R_{s11}. \qquad (12)$$

This is in agreement with the fact that an infinite velocity allows the solid 2 to convect, instantaneously, all of the heat away.

3.2. *Analytical expression of* α

If the ratio $h_i/2B$ ($i = 1$ and 2) is equal to zero, the heat flux is generated at the interface of the real area of contact. In this particular case, the expression of α is given by equation (6). Using equations (10) and (11), one obtains:

$$\alpha = \frac{1}{\left(1 + A\frac{k_2}{k_1}\right)} \qquad (13)$$

where

$$A = \frac{f_1}{(f_{c2}F(V^*))}. \qquad (14)$$

Now if a volume heat generation is considered, another expression for α that involves h_1, h_2, g_1 and g_2 must be found. Consider first the particular case shown Fig. 4b, where the heat flux is not generated on the real contact interface but locally at a certain distance in the solid 2. A mathematical parameter, η_2 that does not rely on any physical considerations is now introduced. η_2 is the ratio of the contact thermal resistance between the real and the fictive interfaces to the contact thermal resistance in the solid 2, R_{s12}. It is similar to equation (6) which was obtained for an interfacial flux generation, makes it possible to derive the following relation for a local internal heat flux generation coefficient $\alpha_2(\eta_2)$:

$$\alpha_2(\eta_2) = \frac{(R_{s12} - \eta_2 R_{s12})}{(R_{s12} + R_{s11})}. \qquad (15)$$

The same consideration for the solid 1 (Fig. 4c) leads to:

$$\alpha_1(\eta_1) = \frac{(R_{s12} + \eta_1 R_{s11})}{(R_{s12} + R_{s11})}. \qquad (16)$$

Since the thermophysical properties are constant, the problem is linear. Thus the superposition of local heat fluxes (Fig. 4b and c) is equivalent to a volume heat flux generation (Fig. 4a) and the integration of equations (15) and (16) over the total friction heat generation volume allows the determination of α:

$$\alpha = \frac{1}{\eta_{m1}} \int_0^{\eta_{m1}} g_1(\eta_1)\alpha_1(\eta_1)\,d\eta_1 + \frac{1}{\eta_{m2}} \int_0^{\eta_{m2}} g_2(\eta_2)\alpha_2(\eta_2)\,d\eta_2 \quad (17)$$

where η_{mi} is the maximum value of η_i. When the flux is generated at the asperities surface, $h_i = 0$ and thus $\eta_{mi} = 0$. The maximum value of η_{mi} is 1, which means that the heat flux is generated within all of the perturbated temperature zone; g_i is a weighting function that represents the distribution of the total friction heat, which implies that:

$$\frac{1}{\eta_{m1}} \int_0^{\eta_{m1}} g_1(\eta_1)\,d\eta_1 + \frac{1}{\eta_{m2}} \int_0^{\eta_{m2}} g_2(\eta_2)\,d\eta_2 = 1. \quad (18)$$

In order to simplify the analysis, it is now supposed that the flux is generated uniformly within the material, thus $g_1(\eta_1) = g$ and $g_2(\eta_2) = 1-g$ and $g \in [0, 1]$. g_1 and g_2 can represent the real distribution of the friction heat if it were known. For example, if the adhesion phenomena is larger than the elastoplastic deformation, then g_1 and g_2 would decrease rapidly with η_1 and η_2, respectively. If g_1 and g_2 are chosen so that the distribution of the friction heat follows a Gaussian curve, then this model gives the same macroscopic results as the one developed by Laraqui [21]. The integration of equation (17) gives:

$$\alpha = \frac{\left(1 + g\dfrac{R_{sl1}}{R_{sl2}}\dfrac{\eta_{m1}}{2} - (1-g)\dfrac{\eta_{m2}}{2}\right)}{\left(1 + \dfrac{R_{sl1}}{R_{sl2}}\right)}. \quad (19)$$

Finally, using equations (10), (11) and (14), the desired expression of the heat generation coefficient is obtained:

$$\alpha = \frac{\left(A\dfrac{\eta_{m1}k_2}{2k_1} + \dfrac{\eta_{m2}}{2}\right)}{\left(1 + A\dfrac{k_2}{k_1}\right)} g + \frac{\left(1 - \dfrac{\eta_{m2}}{2}\right)}{\left(1 + A\dfrac{k_2}{k_1}\right)}. \quad (20)$$

For the interfacial friction heat flux generation case, then $\eta_{m1} = \eta_{m2} = 0$ and equation (20) reduces to equation (13). The analytical solution allows the comparison of p, α and g. First, equation (20) shows that α is a linear function of g. The partition coefficient is defined as $p = \varphi_1/\varphi_g$. An energy balance at the node of temperature θ_1 of the macroscopic model (Fig. 2c) leads to:

$$\varphi_1 = \alpha\varphi_g + \frac{\theta_2 - \theta_1}{R_{sl}}. \quad (21)$$

thus

$$p = \alpha + \frac{\theta_2 - \theta_1}{R_{sl}\varphi_g} \quad (22)$$

which shows that p, α and g are completely different and should not be misleading.

4. NUMERICAL SOLUTION OF THE SLIDING CONTACT MODEL

A numerical solution for the calculation of the temperature fields from the microscopic model is now presented. This solution is not restricted, as the analytical solution, to linear problems or simple geometries. Then a procedure is given to determine, from this numerical solution, the two macroscopic parameters of interest, namely α and R_{sl}.

4.1. *Governing equations and numerical method*

The heat convected away by the sliding solid introduces a transport term in the heat diffusion equation. A volume source term G is used to represent the friction heat flux. The heat diffusion equation and boundary conditions are for solids 1 and 2, respectively:

$$\rho_1 cp_1 \frac{\partial T_1}{\partial t} = k_1 \frac{\partial^2 T_1}{\partial y^2} + k_1 \frac{\partial^2 T_1}{\partial x^2} + G_1(x,y)$$

$$\text{B.C.}\begin{cases} -k_1 \dfrac{\partial T_1}{\partial y} = 0 & y = e_1 - H; \quad x \in [0, 2B-2b] \\ -k_1 \dfrac{\partial T_1}{\partial x} = 0 & y \in]e_1 - H, e_1[; \quad x = 2B - 2b \\ -k_1 \dfrac{\partial T_1}{\partial x} = 0 & y \in]e_1 - H, e_1]; \quad x = 2B \\ -k_1 \dfrac{\partial T_1}{\partial y} = h_{c1}(T_1 - T_{inf1}) & y = 0; \quad x \in [0, 2B] \\ -k_1 \left.\dfrac{\partial T_1}{\partial x}\right|_{x=0} = -k_1 \left.\dfrac{\partial T_1}{\partial x}\right|_{x=2B} & y \in [0, e_1 - H] \end{cases} \quad (23)$$

$$\rho_2 cp_2 \frac{\partial T_2}{\partial t} + \rho_2 cp_2 V \frac{\partial T_2}{\partial x} = k_2 \frac{\partial^2 T_2}{\partial y^2} + k_2 \frac{\partial^2 T_2}{\partial x^2} + G_2(x,y)$$

$$\text{B.C.}\begin{cases} -k_2 \dfrac{\partial T_2}{\partial y} = 0 & y = e_1; \quad x \in [0, 2B-2b[\\ -k_2 \dfrac{\partial T_2}{\partial y} = h_{c2}(T_2 - T_{inf2}) & y = e_1 + e_2; \\ x \in [0, 2B] & \\ -k_2 \left.\dfrac{\partial T_2}{\partial x}\right|_{x=0} = -k_2 \left.\dfrac{\partial T_2}{\partial x}\right|_{x=2B} & y \in [e_1, e_1 + e_2]. \end{cases} \quad (24)$$

The perfect contact equation and the initial condition are:

$$T_1(e_1,y,t) = T_2(e_1,y,t) \quad y \in [2B-2b, 2B]$$
$$T_1(x,y,0) = T_2(x,y,0) = T_0 \forall x \forall y. \tag{25}$$

A finite differences method is used to determine the transient temperature field up to the steady-state regime. The unconditionally stable alternative direction implicit (ADI) scheme is employed to limit the computational time [30]. The classical ADI scheme approximation of the time derivative and the diffusion term are used while the transport term is approximated with the upwind approximation. Such an approximation is valid for large mesh Peclet number.

The ADI method had to be adapted to take into account the periodicity of the system. The two classical steps of the ADI method are thus shortly described.

First step. The intermediate temperature field $T^{k+1/2}$ is computed with an explicit approximation for the heat flux in the y direction and with implicit approximation for all other terms. For $j_1+1 \leqslant j \leqslant j_2-1$, it gives a classical tridiagonal system which can be solved with the Choleski (also called Thomas) method [31]. For $1 \leqslant j \leqslant j_1$ and $j_2 \leqslant j \leqslant j_n$, the periodicity implies the continuity of heat flux densities. It gives rise to a tridiagonal matrix with two supplementary terms equation (26). To avoid the use of an iterative method, this system is split into two tridiagonal subsystems of dimension (i_n-1) which can be solved as usual. This maintains the advantages of the ADI method.

$$\begin{bmatrix} b_1 & c_1 & 0 & 0 & d_1 \\ a_2 & & & & 0 \\ 0 & & & & \\ & & & & 0 \\ 0 & & & & c_{in-1} \\ d_2 & 0 & 0 & a_{in} & b_{in} \end{bmatrix} \begin{bmatrix} T_{1,j}^{k+1/2} \\ \\ \\ \\ \\ T_{in,j}^{k+1/2} \end{bmatrix} = \begin{bmatrix} y_1 \\ \\ \\ \\ \\ y_{in} \end{bmatrix}. \tag{26}$$

Second step. The temperature field T^{k+1} is computed with an explicit approximation for the heat flux in the x direction and implicit approximation for the other terms. Due to the presence of the cavity, when $1 \leqslant i \leqslant i_1-1$, one tridiagonal system must be solved for each solid.

4.2. *Validation and results*

The computer program has been validated by two means. First, a comparison of the temperature field for a zero velocity case was done with a commercial finite element code. Then for non-zero velocities, the heat balance for the steady-state regime was checked. For this study, only steady-state results are of interest. The influence of the convective term is shown on the following test case:

$$2B = 0.6\ \text{mm}; \quad 2b = 0.1\ \text{mm}; \quad e_1 = 0.5\ \text{mm};$$
$$e_2 = 0.4\ \text{mm}; \quad H = 0.1\ \text{mm};$$
$$h_1/2B = h_2/2B = 0.09166;$$
$$h_{c1} = h_{c2} = 100\ \text{W m}^{-2}\text{K}^{-1}; \quad T_{\text{in1}} = T_{\text{in2}} = 0;$$
$$g = 0.5; k_1/k_2 = 1; \quad \varphi_g = 18333.33\ \text{W m}^{-2}.$$

Figures 5 and 6 show the steady-state temperature fields for non-dimensional sliding velocities V^* equal to 0 and 60, respectively. The total friction heat is considered constant to better show the influence of the convective term. An increase of the velocity tends to uniformize the temperature in the x direction in the solid 2, while the solid 1 temperature field is only slightly changed. Note that the temperatures for $y = 0$ and $y = e_1+e_2$ do not vary with x. This means that e_1 and e_2 are big enough, i.e. the zone perturbated by the contact is completely included in the studied volume.

4.3. *Determination of* α *and* R_{sl}

It is now shown how the two macroscopic parameters α and R_{sl}, that were determined analytically, can be calculated from the numerical solution of the microscopic model.

Equation (21) can be recast to get the expression of α:

$$\alpha = \frac{1}{\varphi_g}\left(\varphi_1 - \frac{\theta_2-\theta_1}{R_{sl}}\right) \tag{27}$$

where θ_1 and θ_2 are the extrapolated temperatures at the geometrical interface. An expression of R_{sl} can be obtained from this equation if the imaginary case of a non-zero velocity, but with no friction heat, is considered:

$$R_{sl} = \frac{\theta_2^0-\theta_1^0}{\varphi_1}. \tag{28}$$

For linear problems the values of α and R_{sl} are constants, they only depend on the material properties and contact geometry. Thus, it is possible to determine the two parameters from equations (27) and (28) if the four extrapolated temperatures at the geometrical interface, θ_1, θ_2, θ_1^0 and θ_2^0 are known. For a given geometry, sliding velocity and heat generation parameters, the numerical model is used to compute the steady-state temperature field. From the external surface temperatures T_1 and T_2 and the external surface heat flux densities φ_1 and φ_2, it is possible to calculate the extrapolated temperatures (Fig. 1) at the geometrical interface θ_1 and θ_2:

$$\theta_i = T_i + \varphi_i \frac{e_i}{k_i} \quad i = 1 \text{ or } 2. \tag{29}$$

Thus the numerical determination of α and R_{sl} is very simple since it only requires two independent runs of the computer program. The first one with $\varphi_g = 0$ to calculate θ_1^0 and θ_2^0, the second one with the same parameters but with $\varphi_g \neq 0$ to calculate θ_1 and θ_2.

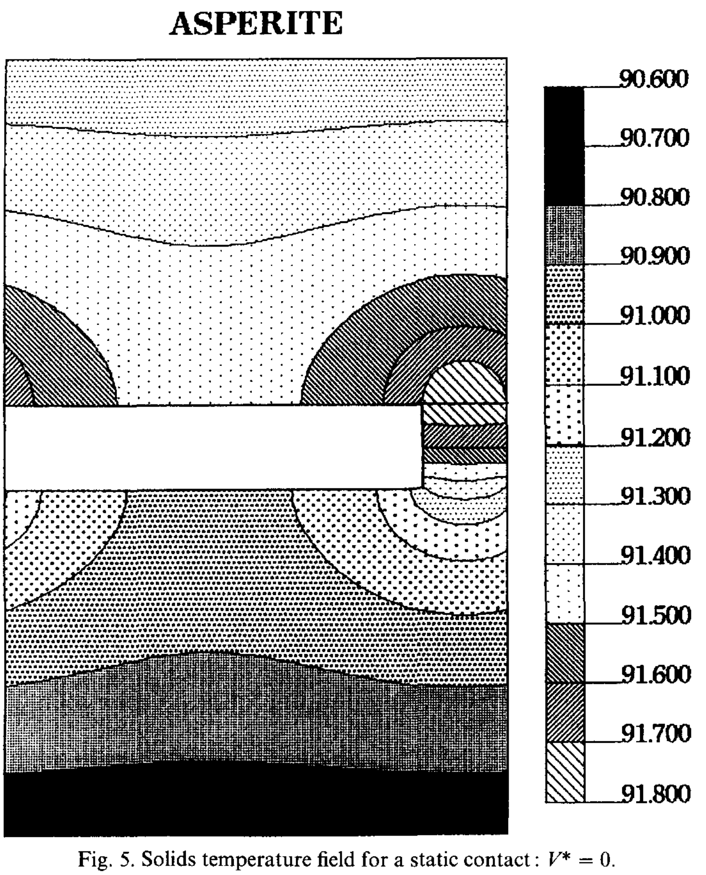

Fig. 5. Solids temperature field for a static contact: $V^* = 0$.

5. NUMERICAL RESULTS

The methodology proposed above for the numerical estimation of α and R_{sl} is now used to perform a sensitivity analysis and is qualitatively validated with the results of the analytical solution.

5.1. *Results for the thermal sliding contact resistances*

Influence of geometry and non-dimensional sliding velocity. The three geometries given in Table 1 are studied. The spacial periodicity $2B$ is the same for the three geometries. The effect of the contact length and the height of the asperity is studied. For the three cases, the variations of R_{sl} vs V_2^* are shown (Fig. 7). It shows that R_{sl} reaches its asymptotic value when V_2^* is around 120. Thus, according to equation (12), $R_{sl1} = R_{sl}(V_2^* = 120)$. From this result and equation (7), R_{sl2} is determined as a function of the non-dimensional sliding speed. As expected from equation (12), R_{sl2} tends to zero when V_2^* tends to infinity. The values of R_{sl1}, which does not depend on the sliding speed, are given in Table 1 for each geometry.

The real contact area for the geometry GE2 is bigger than for the geometry GE1. The heat flux line constrictions are then less important which explains that $R_{sl1}(\text{GE1}) > R_{sl1}(\text{GE2})$. Similarly, the height of the asperity is smaller for the geometry GE3 than for the geometry GE1, thus $R_{sl1}(\text{GE1}) > R_{sl1}(\text{GE3})$. On the other hand, for GE1 and GE3 the contact area is the same which leads to the same constriction in the solid 2 for both cases, consequently $R_{sl2}(\text{GE1}) = R_{sl2}(\text{GE3})$. it is logical to find that R_{sl2} does not depend on the height of the asperity.

Influence of thermophysical properties. To limit the computational time, another set of geometrical parameters has been used in this part. The following geometry was studied: $2B = 1.5$ mm, $2b = 0.5$ mm, $H = 0.5$ mm, $e_1 = e_2 = 2$ mm. The results showed that R_{sl1} does not depend on $\rho_1 cp_1$, k_2 and $\rho_2 cp_2$ and that R_{sl2} does not depend on $\rho_1 cp_1$ and k_1. Figure 8 shows that the variation of R_{sl1} (respectively, R_{sl2}) vs $1/k_1$ (respectively, $1/k_2$) is linear, which is in good agreement with equation (10) (respectively, equation (11)). Note that for R_{sl2} the non-dimensional sliding speed is maintained constant while $\rho_2 cp_2$ and k_2 vary, thus the thermal resistance in the solid 2 depends indirectly on $\rho_2 cp_2$ and its variation function of $1/k_2$ is not strictly linear. Figure 8 confirms that R_{sl2} decreases when the sliding velocity increases, the changes being particularly important for small values of the conductivity.

5.2. *Results for the heat flux generation coefficient*

Influence of geometry and non-dimensional sliding velocity. Three sets of simulation were realized, each one corresponding to the geometry GE1, GE2 and

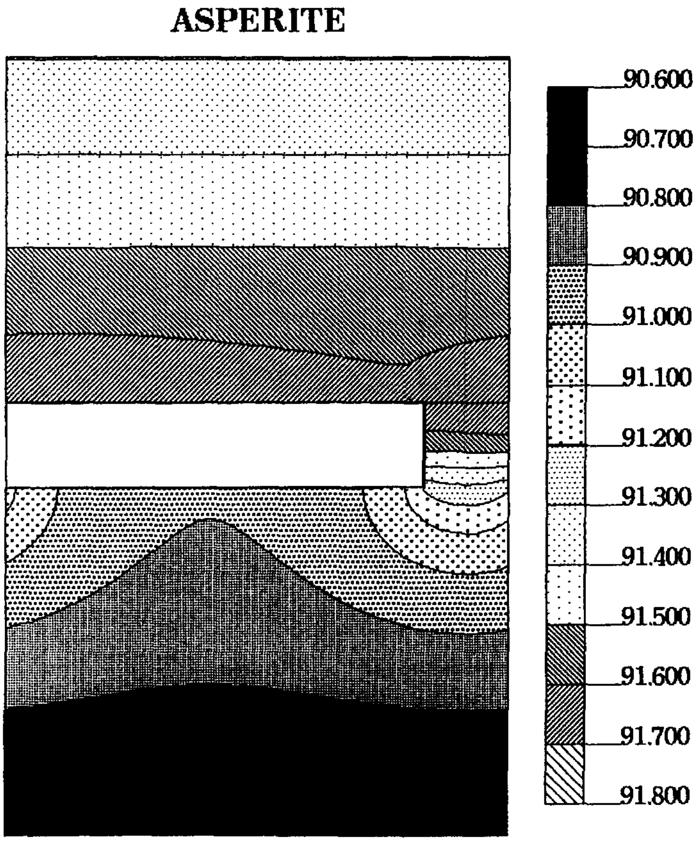

Fig. 6. Solids temperature field for $V^* = 60$.

Table 1. Value of R_{sl1} for different geometries ($2B = 0.6$ mm)

	GE1	GE2	GE3
b/B	1/6	1/4	1/6
$H/2B$	1/6	1/6	1/12
$R^*_{sl1}1000$ (m^2KW^{-1})	0.8213	0.5303	0.6249

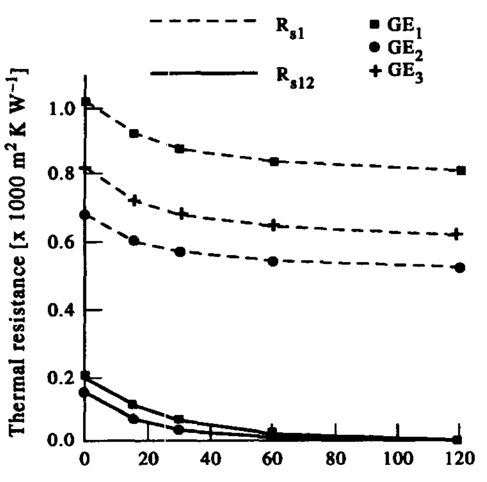

Fig. 7. Total thermal sliding contact resistance and thermal sliding contact resistance in the solid 2 for the three geometries GE1, GE2, GE3.

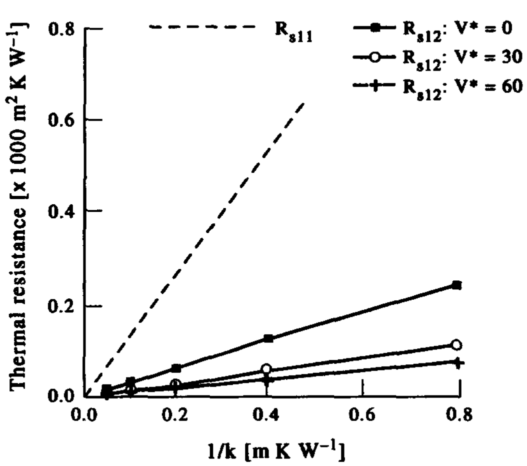

Fig. 8. Thermal contact resistance in the solid 1 (static solid) and in the solid 2 (sliding solid) vs $1/k_1$ and $1/k_2$, respectively.

GE3. For these simulations, $g = 0.25$ and $h/2B = 1/11$. The variations of α vs V^* is shown (Fig. 9). According to its analytical determination, equation (19), α depends on the thermal resistance ratio R_{sl1}/R_{sl2}. For the geometry GE2, the thermal resistances R_{sl1} and R_{sl2} are smaller than for the geometry GE1 but the ratio is nearly constant, so the curves are almost identical. For the geometry GE3, R_{sl1} is smaller, but R_{sl2} is the same, so the ratio is R_{sl1}/R_{sl2}.

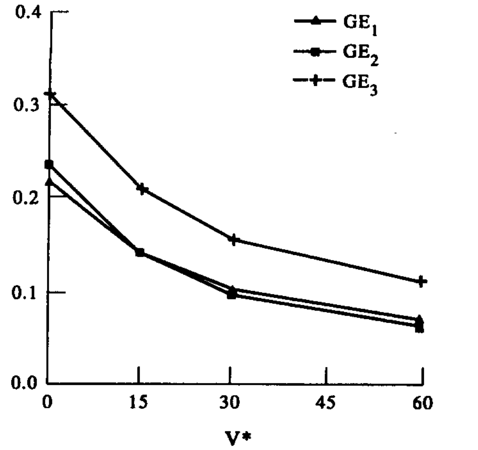

Fig. 9. Heat generation coefficient for the three geometries GE1, GE2, GE3.

This ratio appears in the numerator and denominator of equation (19), but is multiplied by a number less than one in the numerator ($g\eta_{m1}/2$), so α is bigger for the geometry GE3. The same reasoning explains the variation of α with the non-dimensional sliding speed: if V_2^* increases, R_{sl2} becomes smaller, but R_{sl1} remains the same, equation (10), so the ratio R_{sl1}/R_{sl2} is bigger and α decreases. The same trends were obtained for $g = 0.5$ and $g = 0.75$, but as shown below, the value of α depends on g.

Influence of friction heat dissipation parameters. Figure 10 shows, for the geometry GE1, the variations of α vs g for different values of V_2^* and $h/2B (h_1 = h_2 = h)$. The variation of α vs g is linear; the slope of the line increases with $h/2B$ and the ordinate at the origin decreases when V_2^* increases. These results are consistent with equation (20) (η_{m1} and η_{m2} get larger when $h/2B$ increases). As shown in Fig. 11, the variation of α with $h/2B$ depends on g, for small values of g, α barely varies with $h/2B$. If g is big enough, α always increases with $h/2B$ and the variation seems to be linear.

Influence of thermophysical properties. The geometry used to study the influence of the thermophysical properties on R_{sl1} and R_{sl2} was also used in this part. A set of simulations showed that α does not depend on $\rho_1 cp_1$. It varies indirectly with $\rho_2 cp_2$ through V_2^*. The variations of α vs $h/2B$ ($h_1 = h_2 = h$) for different values of k_1/k_2 are shown in Fig. 12 for $V_2^* = 30$ and $g = 0.5$. It is clear that the conductivity ratio has a strong influence on the parameter α. Surprisingly, there is for this case, a value of $h/2B$ for which α does not depend on k_1/k_2. The values of α for $h/2B = 0$ have been calculated using values of R_{sl1} and R_{sl2} obtained from the numerical model and the equation (15) derived from the macroscopic model when the friction heat is generated only at the contact interface. These values are in very good agreement

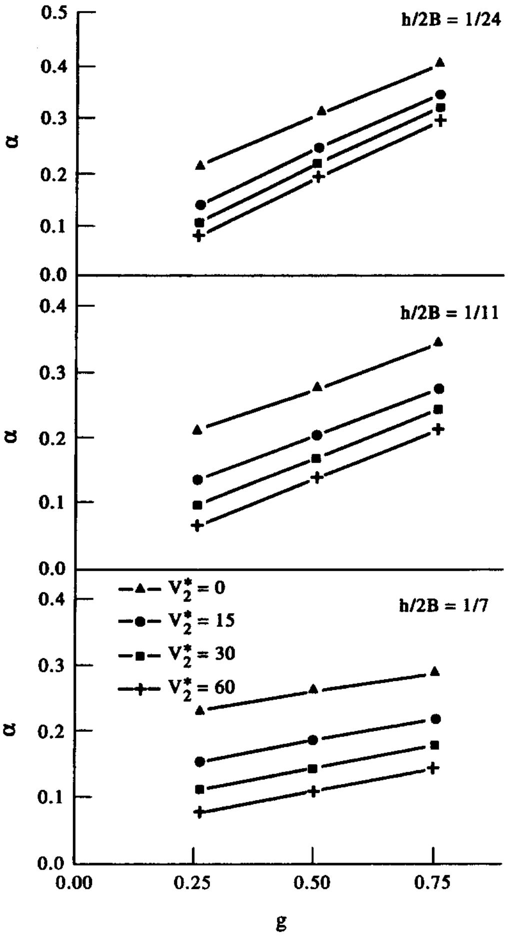

Fig. 10. Heat generation coefficient for various sliding velocities and ratios $h/2B$.

with the limits of the curves when $h/2B$ tends towards zero.

6. CONCLUSIONS

A sliding thermal contact model that accounts for a volume generation of the friction heat has been proposed. This model is based on a microscopic analysis of the heat transfer and heat generation occurring around the contact interface. A numerical procedure that allows one to determine, from this microscopic model, the two parameters of the most established thermal macroscopic model has been developed. This procedure has been qualitatively validated with an analytical solution for the case of a simple contact geometry. However, if a more realistic contact geometry with three-dimensional effects and heat transfer within the contact cavities were considered, then the procedure would still allow one to estimate the macroscopic parameters. It would only require a more powerful numerical code.

Far enough from the interface where the temperature field is not perturbated by the asperities, the results of the microscopic and macroscopic models

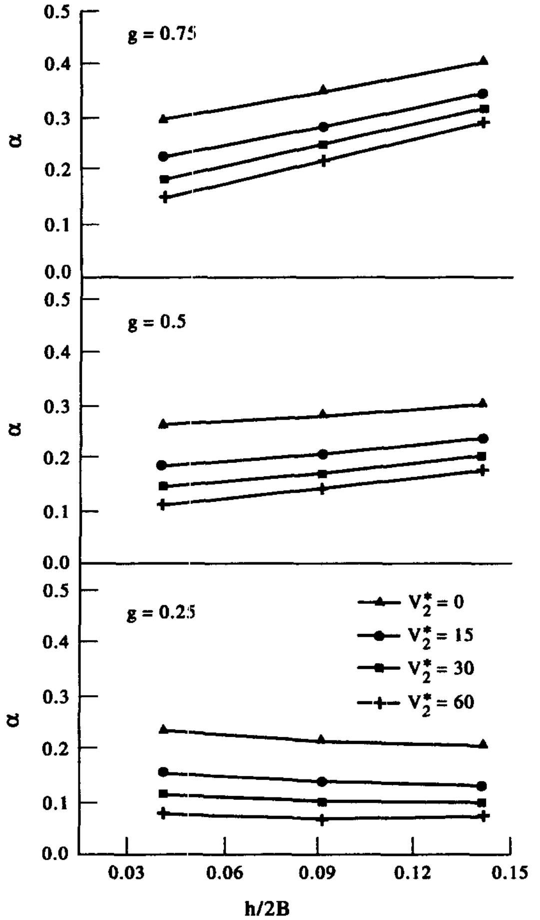

Fig. 11. Heat generation coefficient for various sliding velocities and fractions g.

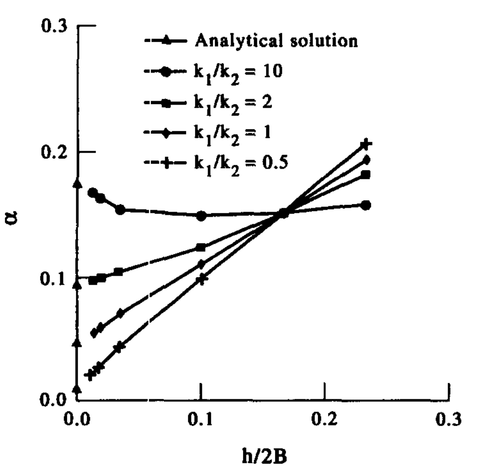

Fig. 12. Heat generation coefficient for various conductivity ratios k_1/k_2.

agree well. It proves that a simple macroscopic model can be used to couple the two solids as long as the temperature variations in the perturbed zone are not of interest. This is true, for example, for large scale engineering problems. However, it requires that the parameters α and R_{sl} are known.

This work showed that α depends greatly on the heat generation distribution in the two solids in the vicinity of the contact interface. The influences of the velocity and the geometry of the asperity on α and R_{sl} have also been shown. For R_{sl}, the same qualitative variations were found as in the experimental study of Vullierme *et al.* [18]. These trends may not be similar for other contact geometries. The analytical solution, even restricted to simple geometries, is very useful in determining the main variations of α and R_{sl} as a function of the many contact parameters. As a matter of fact, it is quite difficult to *a priori* predict the behavior of the macroscopic parameters.

Presently, α and R_{sl} can be determined either experimentally or numerically. The former solution will only allow estimation of the parameters for some specific contact conditions (geometry, material properties, pressure and velocity). On the other hand, the procedure that has been proposed in this paper allows, for any contact geometry and friction heat distribution, the calculation of the two parameters, but it involves friction heat microscopic parameters which are yet unknown. Thus, it emphasizes the need of pursuing research, either experimental (with atomic force microscope for example) or computational (mechanical calculations with a Lagrangian approach), to determine precisely how and where friction is dissipated.

Acknowledgement—This work was supported by GDR 0916 CNES-CNRS-SEP.

REFERENCES

1. Jaeger, J. C., Moving sources of heat and the temperature at sliding contacts, *Proceedings of the Royal Society, New South Wales*, 1942, 203–224.
2. DesRuisseaux, N. R. and Zerkle, R. D., Temperature in semi-infinite and cylindrical bodies subjected to moving heat sources and surfaces cooling. *Journal of Heat Transfer*, 1970, 456–464.
3. Kounas, P. S. and Dimarogonas, A. D., The distribution of friction heat between a stationary pin and a rotating cylinder. *Wear*, 1972, **19,** 415–424.
4. Gecim, B. and Winer, W. O., Steady temperature in rotating cylinder subject to surface heating and convective cooling. *Journal of Tribology, ASME*, 1984, **106,** 120–127.
5. Berry, F. R. and Barber, J. R., The division of frictional heat—a guide to the nature of sliding contact. *Journal of Tribology*, 1984, **106,** 405–415.
6. Dimarogonas, A. D., Heat distribution and flash temperature in radial seals. *Wear*, 1973, **23,** 113–119.
7. Rashid, M. and Seireg, A., Heat partition and transient temperature distribution in layered concentrated contacts, Part II dimensionless relationships and numerical results. *Transactions of the ASME*, 1987, **109,** 496–502.
8. Barber, J. R., An asymptotic solution for short-time transient heat conduction between two similar contacting bodies. *International Journal of Heat Mass Transfer*, 1989, **32,** 943–949.
9. Negus, K. J., Yovanovich, M. M. and Beck, J. V., On the non-dimensionalization of constriction resistance for semi-infinite heat flux tubes. *Journal of Heat Transfer*, 1989, **111,** 804–807.

10. Tio, K. K. and Sadhal, S. S., Thermal constriction resistance: effects of boundary conditions and contact geometries. *International Journal of Heat Mass Transfer*, 1992, **35**, 1533–1544.
11. MacWaid, T. and Marschall, E., Thermal contact resistance across pressed metal contacts in a vacuum environment. *International Journal of Heat Mass Transfer*, 1992, **35**, 2911–2920.
12. Cooper, M. G., Bmikic, B. and Yovanovich, M. M., Thermal contact conductance. *International Journal of Heat Mass Transfer*, 1969, **12**, 279–300.
13. Mal'Kov, V. A., Thermal contact resistance of machined metal surfaces in vacuum environment. *Heat Transfer Soviet Research*, 1970, **2**, 24–30.
14. Bardon, J. P., Contribution à l'étude du transfert de chaleur au contact de deux matériaux. Ph.D. thesis, Faculté des Sciences de l'Université de Poitiers, France. no. 59, 1965.
15. Degiovanni, A. and Moyne, C., Résistance thermique de contact en régime permanent. Influence de la géométrie du contact. *Revue Génerale de Thermique*, 1989, **334**, 557–564.
16. Laurent, M., Contribution à l'étude des échanges de chaleur au contact de deux matériaux. Ph.D. thesis, Faculté des Sciences de l'Université de Lyon, France 1969.
17. Sinicki, J. G., Contribution à la mesure de résistances thermiques de contact en régime transitoire. Ph.D. thesis, Université Claude Bernard Lyon, France, 1975.
18. Vullierme, J. J., Lagarde, J. J. and Cordier, H., Etude de la résistance de contact entre deux matériaux en frottement—influence de la vitesse relative de glissement. *Int. J. Heat Mass Transfer*, 1992, **22**, 1209–1219.
19. Badie-Levet, D., Les paramètres thermiques du frottement sec métal–matière plastique. Recherche des champs de température dans les corps en mouvement relatif pour une condition de contact imparfait: application aux paliers. Ph.D. thesis, Université de Nantes, France, 1985.
20. Bardon, J. P., Bases physiques des conditions de contact thermique imparfait entre milieu en glissement relatif. *Revue Générale de Thermique*, 1994, 85–92.
21. Laraqui, N., Température de contact et coefficient de partage de flux généré par frottement sec entre deux solides. Approche nouvelle de la génération de flux. *International Journal of Heat Mass Transfer*, 1992, **35**, 3131–3141.
22. Kennedy, Thermal and thermomechanical effect in dry sliding. *Wear*, 1984, **100**, 453–476.
23. Sadhal, S. S., Unsteady heat flow between solids with partially contacting interface. *Transactions of the ASME*, 1981, **103**, 32–35.
24. Bardon, J. P., Personal communication.
25. Bardon, J. P., Introduction à l'étude des résistances thermiques de contact. *Revue Générale de Thermique*, 1972, **125**, 429.
26. Yovanovich, M., Cordier, H. and Coutenceau, J., Sur la résistance thermique due à un contact unique de section circulaire. *Comptes-Rendus de l'Academie de Sciences Paris*, 1969, **268**, B-1.
27. Bardon, J. P. and Cordier, H., Etude du mécanisme de passage de la chaleur au contact de solides accolés. *Comptes-Rendus de l'Academie de Sciences, Paris*, 1966, **262**, 322–325.
28. Carslaw and Jaeger, In *Heat Conduction in Solid*, 2nd edn. Oxford University Press, Oxford, 1959, pp. 214–217.
29. Yovanovich, M., Thermal constriction resistance between contacting metallic paraboloid. Application to instrument bearings. Progression aeronautic and astronautics. *Heat Transfer and Space Craft Thermal Control*, 1971, **24**, 337–358.
30. Lapidus, L. and Pinder, G. F. *Numerical Solution of Partial Differential Equations in Science and Engineering*. Wiley, New York, 1982.
31. Nougier, J. P., *Méthodes de calcul numériques*. Masson, Paris, 1987.